Imaging Agents

DOI: 10.1002/anie.201102892

Tumor-Targeting Gold Particles for Dual Computed Tomography/Optical Cancer Imaging**

In-Cheol Sun, Dae-Kyung Eun, Heebeom Koo, Chang-Yong Ko, Han-Sung Kim, Dong Kee Yi, Kuiwon Choi, Ick Chan Kwon, Kwangmeyung Kim, and Cheol-Hee Ahn**

In memory of Tae Gwan Park

Nanotechnology and molecular imaging have been combined to generate multimodal imaging technology that consists of more than two imaging functions combined in one imaging probe.[1] However, the simple combination of different imaging modalities is not innovative. Ideal multiimaging modality should be synergistically combined to provide unique imaging information, which can overcome its own weak point of each imaging modality. Recently, various nanoparticles based on quantum dots,[2] polymers,[3] and metals[4] have been widely applied to biomedical imaging probes. In particular, gold nanoparticles (AuNPs) have been paid much attention in the molecular-imaging field because of their unique characteristics, such as easy fabrication, controllable size and shapes, biocompatibilty, and fluorescence quenching effect. Furthermore, AuNPs may be suitable for computed tomography (CT) imaging owing to their high X-ray absorption coefficient.

However, in vivo applications of bare AuNPs are very limited, mainly because of their low stability and lack of target-cell specificity. For clinical applications, their stability should be guaranteed firstly by surface modification with biocompatible and anti-biofouling materials. For example, thiolated polyethylene glycols (PEGs) have been introduced for the surface coating of AuNPs, but they are unstable at elevated temperature or high salt concentration or in the presence of biological reducing agents (e.g., dithiothreitol and glutathione).[5] In addition, PEG on the AuNP surface prevents its cellular uptake, which causes a negative effect on high accumulation in target sites such as tumor tissues.[6] Therefore, a simple and versatile surface-modification strategy is an urgent challenge for developing ideal AuNP-based imaging probes for multimodal imaging.

Herein, we report tumor targeting AuNP nanoprobes for dual CT/optical imaging of cancer (Scheme 1). First, to make physiologically stable and tumor-targeting AuNPs as a CT contrast probe, AuNPs were modified with glycol chitosan (GC) polymers (GC-AuNPs). It has been reported that GC-based nanoparticles show excellent stability and tumor-targeting ability by the enhanced permeation retention (EPR) effect.[7] Second, for the fluorescence optical imaging, matrix metalloproteinase (MMP) activatable peptide probes were chemically conjugated to GC-AuNPs, resulting in MMP-GC-AuNPs. Previously, gelatin/QD nanoparticles were reported for enhanced tumor penetration by peptide degradation by MMP.[2] Based on similar degradation of peptide-specific probes, we developed MMP-specific fluorescent nanoparticles, wherein the near-infrared fluorecence (NIRF) of MMP-GC-AuNPs was strongly quenched by the combinational quenching effects between organic black hole quencher and gold particle surface.[8] However, the quenched

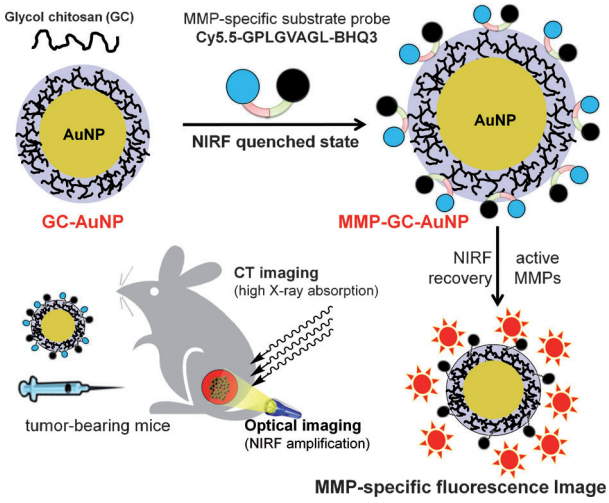

Scheme 1. Schematic diagram of GC coated (GC-AuNPs) and MMP peptide probe conjugated gold nanoparticles (MMP-GC-AuNPs) as multimodal CT/optical imaging probes for cancer imaging.

[*] I. C. Sun, Dr. H. Koo, Dr. K. Choi, Dr. I. C. Kwon, Dr. K. Kim
Center for Theragnosis, Biomedical Research Institute
Korea Institute of Science and Technology
39-1 Hawolgok-dong, Seongbuk-gu, Seoul 136-791 (Korea)
E-mail: kim@kist.re.kr
D. K. Eun, Dr. C. H. Ahn
Research Institute of Advanced Materials (RIAM), Department of Materials Science and Engineering, Seoul National University
San 56-1, Sillim, Gwanak, Seoul, 151-744 (Korea)
E-mail: chahn@snu.ac.kr
Dr. C. Y. Ko, Dr. H. S. Kim
Department of Biomedical Engineering, Yonsei Univeristy
Wonju, Ganwondo 220-710 (Korea)
Dr. D. K. Yi
Division of Bionanotechnology, Gachon Bionano Institute
Kyungwon University, Geonggi-do, 461-701 (Korea)

[**] We thank the late Prof. Tae Gwan Park for valuable discussion about this research. This work was financially supported by the Real-Time Molecular Imaging Project, GRL Program of MEST, Intramural Research Program of KIST, M.D.-Ph.D. Program (2010-0019863, 2010-0019864), and the Basic Science Research Program (2010-0027955) of MEST.

Supporting information for this article is available on the WWW under http://dx.doi.org/10.1002/anie.201102892.

NIRF was recovered by cleavage of the peptide substrates upon exposure to the active MMPs, which is overexpressed in tumor tissue.[4] Therefore, we expect that this gold nanoparticle-based CT/optical dual imaging probe may simultaneously provide CT images with high spatial resolution and optical images with high sensitivity.

To demonstrate our rationale, the GC-AuNPs were firstly prepared by using GC as reducing and stabilizing agent simultaneously in the process of $H[AuCl_4]$ reduction.[9] Under optimum reaction conditions, the weight ratio of GC polymers in the GC-AuNPs was measured to 11.7 wt%, quantified by thermogravimetric analysis (TGA). This result suggests that many GC polymers can strongly absorb on the AuNP surface owing to the multiple binding of primary amines of GC polymers to the AuNP surface even in the presence of salt.[10] Secondly, an MMP activatable peptide probe was synthesized by standard solid-phase Fmoc peptide chemistry as previously described.[4] The NIRF dye (Cy5.5) and black hole quencher (BHQ) were coupled to both ends of MMP cleavable peptide substrate, resulting Cy5.5-Gly-*Pro-Leu-Gly-Val-Arg*-Gly-Lys(BHQ)-Gly-Gly, which is used as the MMP-2 specific substrate (the cleavable site indicated by italics, see the Supporting Information for details). The freshly prepared MMP peptide probe was successfully conjugated onto the GC-AuNPs in the presence of EDC and NHS as catalysts. The final products were denoted as MMP-GC-AuNPs (see Figure S1 in the Supporting Information). After dissolving of MMP-GC-AuNPs in KCN solution, we estimated that 572 molecules of MMP peptide probes were chemically conjugated onto each GC-AuNP, confirmed by the absorption curve of Cy5.5 at 675 nm.

The UV/Vis spectra of GC-AuNPs and MMP-GC-AuNPs indicated that the surface plasmon resonance (SPR) peaks at 536 nm were not changed after chemical modification, compared with those of bare AuNPs produced with sodium citrate (Figure 1a).[11] The stability and morphology of MMP-GC-AuNPs were further confirmed through TEM images in which they showed well-dispersion and spherical shapes with diameter of 20 nm (Figure 1b). A uniform GC layer with thickness of about 10 nm was shown on the surface of nanoparticles (white arrows), the hydrodynamic diameter measured with dynamic light scattering (DLS) in aqueous condition increased to 99.4 ± 16.8 nm (Figure 1c) owing to the large hydrodynamic volume of glycol chitosan.[12] The positive value of the ζ potential (34.48 ± 1.00 mV) also supported the existence of primary amine groups of GC on the surface, which was contrary to negative value (-26.0 ± 0.4 mV) of sodium citrate AuNPs.[13] Importantly, MMP-GC-AuNPs were very stable in both distilled water and PBS buffer at different pH values (pH 3–11) and their diameter was preserved for up to 80 days, but bare gold particles immediately precipitated in PBS buffer (Figure 1d,e and Figure S2). The cytotoxicity of MMP-GC-AuNPs was also examined by MTT assay (MTT = 3-(4,5-dimethylthiazol-2-yl)2,5-diphenyltetrazolium bromide). They showed biocompatibility even in high concentrations of up to 1 mg mL^{-1} (Figure 1f).

Prior to in vivo multimodal imaging studies, first, the X-ray absorption of MMP-GC-AuNPs was compared to that of

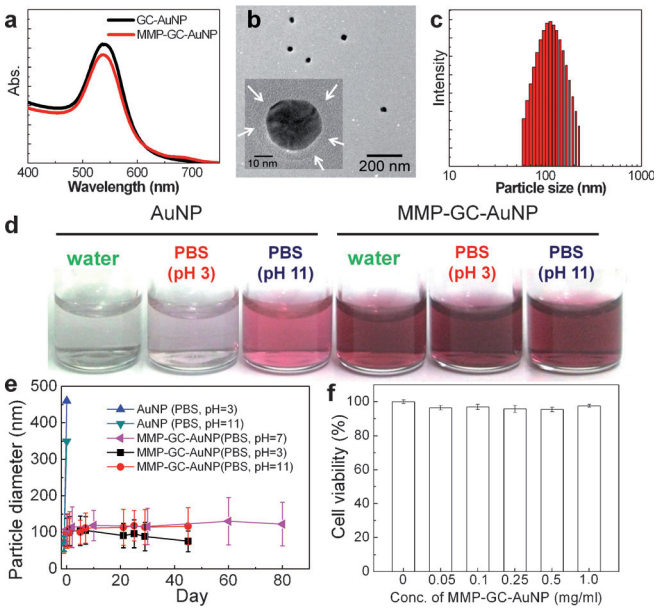

Figure 1. a) UV/Vis absorption spectra of GC-AuNPs and MMP-GC-AuNPs. b) TEM images and c) size distribution of MMP-GC-AuNPs. d) Optical images and e) particle size for 80 days of MMP-GC-AuNPs in water or PBS buffer at various pH values. f) HeLa cell viability after 24 h of incubation with increasing concentration of MMP-GC-AuNPs (0.05 mg mL^{-1} = 7×10^{11} particles mL^{-1}) using MTT assay.

commercial iodine-based contrast agent (eXIA^{TM}160) in phantom CT images. As expected, enhanced contrast was achieved with MMP-GC-AuNPs, whose X-ray absorption was visualized as a white spot in the phantom CT images (Figure 2a). The imaging also revealed linear increments

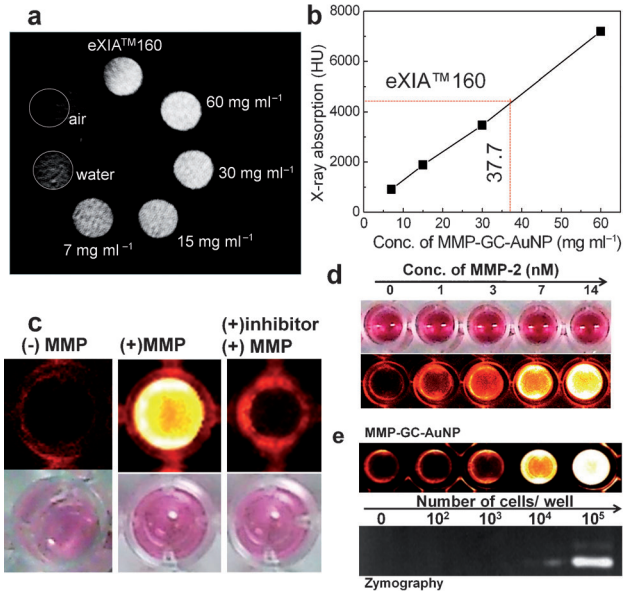

Figure 2. a) MicroCT image of MMP-GC-AuNPs and b) their X-ray absorption (HU). c,d) NIRF and bright image of MMP-GC-AuNPs in 96-well plate containing c) MMP or its inhibitor and d) various concentrations of MMP-2 after incubation (60 min, 37°C). e) NIRF image and zymography of cell culture media containing MMP-GC-AuNPs.

according to the concentration of the MMP-GC-AuNPs; 37.7 mg mL^{-1} of nanoparticles gave an equivalent Hounsfield units (HU) value with eXIA™160 (corresponding to 160 mg I mL^{-1}) (Figure 2b). This result explicitly indicated that the X-ray absorption of the MMP-GC-AuNPs was 4.2 times higher than that of eXIA™160 at the same elemental concentration.

Second, fluorescence recovery of MMP-GC-AuNPs as an optical imaging probe was also examined. The NIRF intensity of Cy5.5 labeled MMP peptide probe substrate was strongly quenched by 90% by fluorescence resonance energy transfer (FRET) of black hole quencher (BHQ; Figure S3).[8a] In addition, the gold particle surface further quenched the MMP-GC-AuNPs by about 95% compared to free Cy5.5-MMP peptide probe, because of the surface-energy-transfer properties of AuNPs.[8b] In Figure 2c, the quenched state and recovered NIRF of MMP-GC-AuNPs were visualized before and after the exposure to MMP; the significant amplification of NIRF intensity was observed only in the absence of MMP inhibition. In addition, the NIRF increased according to MMP-2 enzyme concentrations (1–15 nM; Figure 2d) and NIRF recovery was observed at low concentration (25–50 μg mL^{-1}) of MMP-GC-AuNPs (Figure S4). This showed sensitivity and specificity of our probe against MMP. Also the high-sensitivity of MMP-GC-AuNPs was shown through activity test with MMP enzymes secreted from the SCC-7 cell line. Importantly, the strong NIRF signals from the well containing only 10^4 cells showed high sensitivity against MMP enzymes, which was not observed in the zymography (Figure 2d).[14]

Based on these encouraging in vitro results, we performed in vivo dual CT/optical imaging studies with MMP-2 positive HT-29 tumor bearing mouse model.[15] First, the potential of MMP-GC-AuNPs as in vivo CT contrast probes weas examined. Because of their excellent stability and biocompatibility, our gold particles could be injected intravenously into the mice at high concentration (200 μL, 300 mg kg^{-1}). However, bare AuNPs presented rapid aggregation at this concentration and could not be injected. As shown in Figure 3a, tumor tissue was able to be delineated from the surrounding tissues after 2 h post-injection. In particular, after 24 h post-injection, the HU value in the tumor tissue increased about fivefold (HU = 254) relative to normal tissue. The enhanced stability of MMP-GC-AuNPs enabled long circulation in the body, which facilitated targeting to the tumor through the EPR effect. Furthermore, detailed anatomical information could be acquired from the three-dimensional reconstructed images in which the exact shape of the tumor tissue was clearly visualized. In contrast, tumor imaging was impossible with eXIA™160 because of its rapid clearance from the body and the lack of tumor targeting properties (data not shown).

Second, the in vivo optical imaging ability of MMP-GC-AuNPs was also evaluated in the same HT-29 tumor bearing mouse. After intravenous injection of MMP-GC-AuNPs (200 μL, 5 mg kg^{-1}), the increased NIRF signal was observed only in the tumor region beginning in 1 h of post-injection (Figure 3b). Tumor location was easily identified with maximum NIRF signal in 4 h, which was maintained up for 48 h (data not shown). However, NIRF was not recovered when

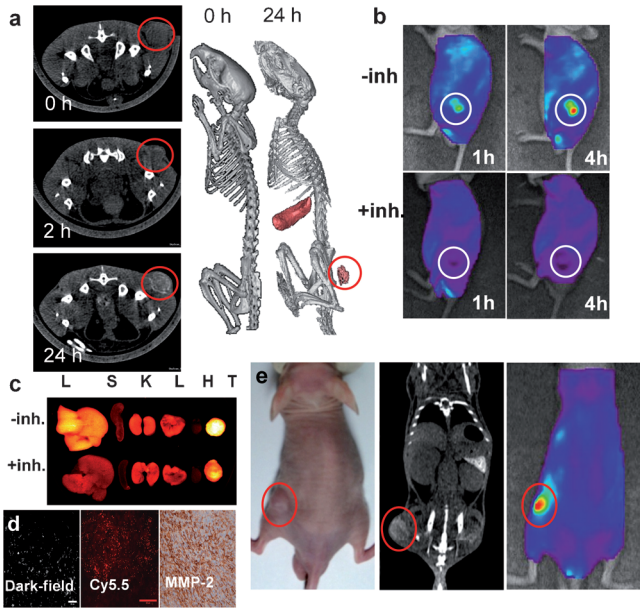

Figure 3. a) Cross-sectional CT images of tumor before (0 h) and after (2 h, 24 h) tail-vein injection of GC-AuNPs and their 3D reconstructed images. b) NIRF tomographic images of HT-29 tumor-bearing mice after injection of the MMP-GC-AuNPs with and without inhibitor (blue: low intensity, red: high intensity). c) NIRF images of their organs. The organs were excised 4 h post-injection. L: liver, S: spleen, K: kidney, L: lung, H: heart, T: tumor. d) Dark-field (left), fluorescence (middle), and MMP-2 enzyme stained (right) microscopic images of excised HT-29 tumor tissue. Scale bar indicates 50 μm. e) Dual CT/optical imaging of the same HT-29 tumor-bearing mouse model 24 h post-injection.

the MMP inhibitor was administered intratumorally 30 min prior to the injection of the MMP-GC-AuNPs. To prove that the NIRF signal originated from the specificity of MMP-GC-AuNPs against target MMP activity, the mice were dissected for histological analysis. The NIRF of tumor was substantially distinguishable from that of other organs or inhibitor-treated ones (Figure 3c). Also, low uptake of MMP-GC-AuNPs in the liver was observed proving the role of glycol chitosan for inhibition of unintended uptake from macrophages and aggregation.[7b] In addition, in the sliced tumor specimens, we confirmed the existence of MMP-GC-AuNPs with dark-field microscopic images, NIRF signal, and antibody-stained MMP enzymes with optical fluorescence microscopy (Figure 3d). However, when the inhibitor was treated, the NIRF signal was not detected because of the inhibition of MMP activity even though nanoparticles were discovered in the dark-field images (Figure S5). Based on those results, we showed that MMP-GC-AuNPs were efficiently accumulated in the tumor tissue and their NIRF was recovered sensitively by MMP enzymes. Finally, our gold particle based imaging probe imaged the tumor tissue using CT and optical imaging simultaneously at the same tumor-bearing mouse model (Figure 3e). It provided accurate anatomical data of the tumor as well as MMP-dependent biological information, simultaneously. Therefore, our MMP-GC-AuNP probes with biocompatible polymer coating showed its potential as a target-molecule-specific, dual CT/optical imaging probe for cancer imaging. In further work, the tumor targeting efficacy

of AuNP-based imaging probe needs to be improved to synchronize the injection dose of dual imaging probe for CT/optical dual cancer imaging.

Received: April 27, 2011
Revised: June 29, 2011
Published online: August 26, 2011

Keywords: computed tomography · gold · imaging agents · nanoparticles

[1] S. Lehmann, D. P. Stiehl, M. Honer, M. Dominietto, R. Keist, I. Kotevic, K. Wollenick, S. Ametamey, R. H. Wenger, M. Rudin, *Proc. Natl. Acad. Sci. USA* **2009**, *106*, 14004 – 14009.
[2] C. Wong, T. Stylianopoulos, J. Cui, J. Martin, V. P. Chauhan, W. Jiang, Z. Popovic, R. K. Jain, M. G. Bawendi, D. Fukumura, *Proc. Natl. Acad. Sci. USA* **2011**, *108*, 2426 – 2431.
[3] K. Kim, M. Lee, H. Park, J. H. Kim, S. Kim, H. Chung, K. Choi, I. S. Kim, B. L. Seong, I. C. Kwon, *J. Am. Chem. Soc.* **2006**, *128*, 3490 – 3491.
[4] S. Lee, E. J. Cha, K. Park, S. Y. Lee, J. K. Hong, I. C. Sun, S. Y. Kim, K. Choi, I. C. Kwon, K. Kim, C. H. Ahn, *Angew. Chem.* **2008**, *120*, 2846 – 2849; *Angew. Chem. Int. Ed.* **2008**, *47*, 2804 – 2807.
[5] a) Z. Li, R. C. Jin, C. A. Mirkin, R. L. Letsinger, *Nucleic Acids Res.* **2002**, *30*, 1558 – 1562; b) R. L. Letsinger, R. Elghanian, G. Viswanadham, C. A. Mirkin, *Bioconjugate Chem.* **2000**, *11*, 289 – 291.
[6] J. X. Cheng, T. B. Huff, M. N. Hansen, Y. Zhao, A. Wei, *Langmuir* **2007**, *23*, 1596 – 1599.
[7] a) K. Kim, J. H. Kim, H. Park, Y. S. Kim, K. Park, H. Nam, S. Lee, J. H. Park, R. W. Park, I. S. Kim, K. Choi, S. Y. Kim, I. C. Kwon, *J. Controlled Release* **2010**, *146*, 219 – 227; b) J. H. Na, H. Koo, S. Lee, K. H. Min, K. Park, H. Yoo, S. H. Lee, J. H. Park, I. C. Kwon, S. Y. Jeong, K. Kim, *Biomaterials* **2011**, *32*, 5252 – 5261.
[8] a) S. A. E. Marras, F. R. Kramer, S. Tyagi, *Nucleic Acids Res.* **2002**, *30*, e122; b) B. Dubertret, M. Calame, A. J. Libchaber, *Nat. Biotechnol.* **2001**, *19*, 365 – 370.
[9] D. R. Bhumkar, H. M. Joshi, M. Sastry, V. B. Pokharkar, *Pharm. Res.* **2007**, *24*, 1415 – 1426.
[10] R. Levy, N. T. K. Thanh, R. C. Doty, I. Hussain, R. J. Nichols, D. J. Schiffrin, M. Brust, D. G. Fernig, *J. Am. Chem. Soc.* **2004**, *126*, 10076 – 10084.
[11] T. J. Norman, C. D. Grant, D. Magana, J. Z. Zhang, J. Liu, D. L. Cao, F. Bridges, A. Van Buuren, *J. Phys. Chem. A J. Phys. Chem. B.* **2002**, *106*, 7005 – 7012.
[12] K. G. H. Desai, H. J. Park, *Drug Dev. Res.* **2005**, *64*, 114 – 128.
[13] S. H. Brewer, W. R. Glomm, M. C. Johnson, M. K. Knag, S. Franzen, *Langmuir* **2005**, *21*, 9303 – 9307.
[14] a) M. Schwab, in *Encyclopedic Reference of Cancer* (Ed.: M. S. Stack), Springer-Verlag, Berlin, **2001**, pp. 530 – 535; b) T. M. Leber, F. R. Balkwill, *Anal. Biochem.* **1997**, *249*, 24 – 28.
[15] E. Roeb, C. G. Dietrich, R. Winograd, M. Arndt, B. Breuer, J. Fass, V. Schumpelick, S. Matern, *Cancer* **2001**, *92*, 2680 – 2691.

